GLOBAL BIOGEOCHEMICAL CYCLES, VOL. 10, NO. 3, PAGES 527–541, SEPTEMBER 1996

Calcite dissolution in sediments of the Ontong-Java Plateau: In situ measurements of pore water O_2 and *p*H

Burke Hales

Lamont-Doherty Earth Observatory of Columbia University, Palisades, New York

Steve Emerson

School of Oceanography, University of Washington, Seattle

Abstract. We present in situ electrode measurements of sediment resistivity, pore water oxygen, and pore water *p*H from three stations between 2300 and 3000 m depth on the Ontong-Java Plateau in the western equatorial Pacific. One of these stations is also the site of a concurrent benthic chamber incubation experiment [Jahnke *et al.*, 1994]. The pore water oxygen data and a steady state diffusion and reaction model constrain the depth-dependent rate of oxic respiration in the sediments and imply a diffusive flux of oxygen to the sediments of 10-21 μmol cm^{-2} yr^{-1}. Given these respiration rates, the pore water *p*H data cannot be explained without calcite dissolution driven by metabolically produced CO_2. The dissolution necessary to explain the observations, quantified by a statistical approach, is 3.5-6 μmol cm^{-2} yr^{-1}, which corresponds to at least 20-40% of the calcite rain to these sediments. Over 65% of the total dissolution is driven by metabolic CO_2. Oxygen fluxes and net calcite dissolution constrained by the electrode data are compatible with the benthic chamber measurements of *Jahnke et al.* [1994]. The dissolution flux, while a significant part of the early diagenesis of calcite in these sediments, is less than would be predicted by earlier models of dissolution, and *Jahnke et al.* [1994] probably could not distinguish it from zero with the benthic chamber technique. The dissolution rates found in this study are lower than previous estimates because the respiration reaction is concentrated near the sediment-water interface, and the calcite dissolution rate constants are very small. The statistical evaluation of the pore water *p*H data and model constrain the calcite dissolution rate constant to 0.005-0.16% d^{-1}, following the general trend of lower values determined by in situ techniques rather than by laboratory methods.

Introduction

We describe a study of the early diagenesis of organic carbon and calcium carbonate in pelagic sediments of the western equatorial Pacific. Our goals were (1) to determine the total respiration and dissolution fluxes within the sediments and compare them to the rates of supply to, and burial within, the sediments; (2) to separate the effects on calcium carbonate dissolution due to bottom water undersaturation from those due to metabolic addition of CO_2 within the sediments; and (3) to determine the empirical forms of the kinetics of these reactions within the sediments.

Understanding the mechanism of calcite dissolution is critical because the balance between the influx of alkalinity from rivers and the loss by oceanic burial of calcium carbonate can determine the CO_2 partial pressure (P_{CO2}) of the surface waters and hence of the atmosphere on glacial timescales [*Archer and Maier-Reimer*, 1994; *Emerson and Archer*, 1992; *Broecker*, 1989; *Boyle*, 1988; *Broecker and Peng*, 1987]. *Archer and Maier-Reimer* [1994] argued that dissolution in pelagic sediments driven by metabolically produced CO_2 can drive atmospheric CO_2 differences between glacial and interglacial periods if the ratio of the supply rates of organic carbon and calcite to the sediments changed over those timescales. It is clear that calcium carbonate accumulation in the sediments is linked to glacial cycles [e.g., *Farrell and Prell*, 1989]; however, separating the effects of dissolution (either due to bottom water saturation state changes or increased supply of organic matter to the sediments) from changes in productivity is difficult without quantification of the kinetics of dissolution.

These are not new questions, but there is a fair amount of disagreement between historical attempts to answer them. *Emerson and Bender* [1981] first quantified the amount of calcite that could dissolve in sediments in response to metabolically produced CO_2. Subsequent in situ *p*H electrode measurements in pore waters of sediments [*Archer et al.*, 1989; *Hales et al.*, 1994; *Cai et al.*, 1995] both above and below the saturation horizon could not be explained without dissolution in response to metabolically produced CO_2. Studies of pore water chemistry, measured in pore waters collected with in situ samplers, also implicated dissolution driven by metabolic CO_2 [*Sayles*, 1980, 1985; *Sayles and Curry*, 1988; *Martin and Sayles*, 1996]. Bulk sediment calcite content and sediment dissolution indices based on foraminiferal assemblages, however, often do not show significant changes above the depth of the saturation horizon

Paper Number 96GB01522.
0886-6236/96/96GB-01522$12.00

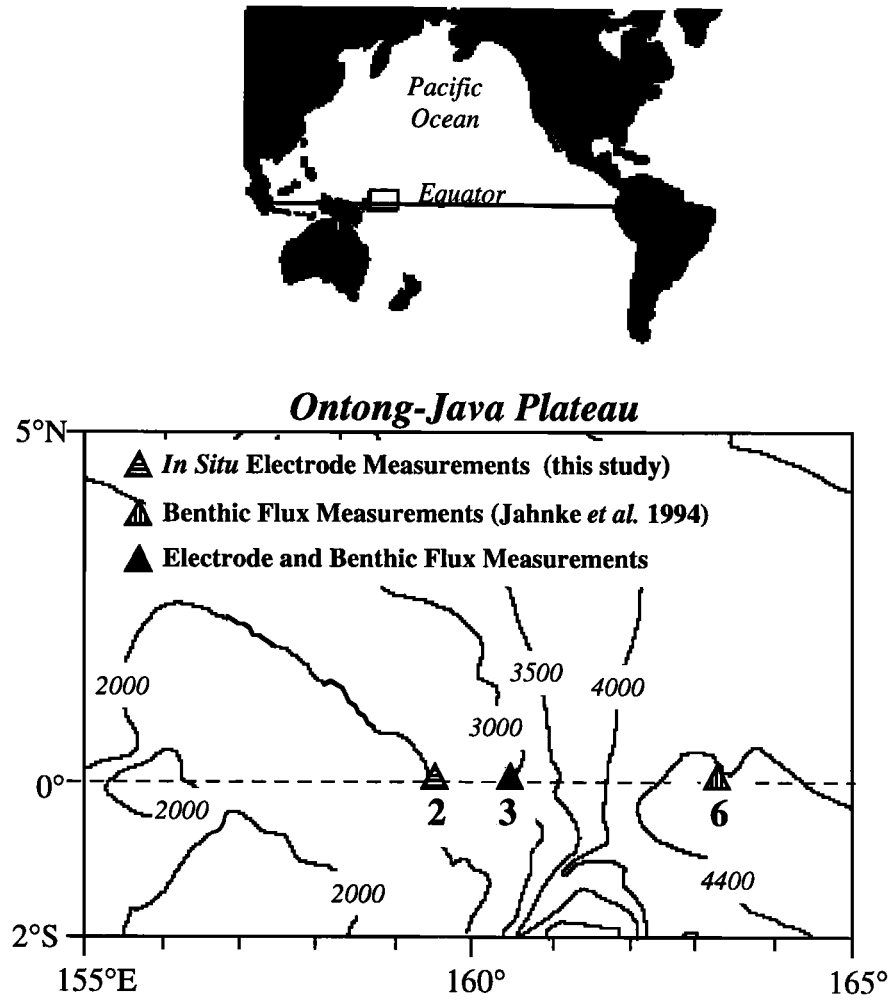

Figure 1. Map of the Ontong-Java Plateau study area. Depth contours in meters.

[*Berger et al.*, 1982]. *Jahnke et al.* [1994], based on direct measurements of calcium and alkalinity fluxes at the seafloor, questioned earlier estimates of metabolic dissolution. They found significant alkalinity and calcium fluxes out of sediments at depths below the saturation horizon but none from depths near or above the saturation horizon. Fluxes predicted with respiration and dissolution rate models used previously [*Emerson and Bender*, 1981; *Archer et al.*, 1989; *Archer and Maier-Reimer*, 1994] were significantly greater than the benthic chamber measurements, while models including dissolution driven only by bottom water undersaturation were in agreement with these observations.

The rate of calcium carbonate dissolution in seawater $R_{d,C}$ is given by the empirical expression:

$$R_{d,C} = k_{d,C}[CaCO_{3(s)}](1-\Omega_C)^{n_C} \quad (1)$$

[*Keir*, 1980; *Morse*, 1978; *Walter and Morse*, 1985]. The saturation state of the surrounding water with respect to calcite Ω_C is defined by

$$\Omega_C \equiv \frac{[Ca^{2+}][CO_3^{2-}]}{K_{sp,C}}, \quad (2)$$

where $K_{sp,C}$ is the thermodynamic solubility of calcite [UNESCO, 1987]. The rate constant $k_{d,C}$ and the reaction order n_C are determined empirically. Field studies of calcite dissolution have generally assumed that the exponent, n_C, is 4.5 [*Archer et al.*, 1989; *Hales et al.*, 1994; *Jahnke et al.*, 1994; *Berelson et al.*, 1994; *Cai et al.*, 1995; *Martin and Sayles*, 1996], following *Keir* [1980], although other laboratory studies have shown that n_C may be as low as 2 [*Walter and Morse*, 1985]. There is less agreement about the value of $k_{d,C}$. *Keir* [1980] performed laboratory measurements of the rate of dissolution of several different kinds of natural and synthetic calcite, finding that the best value for bulk sediment was at least 1000% d^{-1}, which appears to be in accord with the ^{14}C ages of the mixed layers of deep pelagic carbonate sediments [*Keir and Michel*, 1993]. Determinations of $k_{d,C}$ based on field data generally have yielded much lower values. Measurements of in situ benthic fluxes [*Jahnke et al.*, 1994; *Berelson et al.*, 1994], in situ microelectrode pore water *p*H profiles [*Archer et al.*, 1989; *Cai et al.*, 1995; *Hales et al.*, 1994], or carbonate chemistry of pore waters collected with in situ samplers [*Martin and Sayles*, 1996], interpreted with models of the pore water reactions, give estimates of $k_{d,C}$ from 0.2 to 100 % d^{-1}.

Table 1. Ontong-Java Plateau Station Descriptions

Station	Depth, m	Bottom Water Properties			
		Oxygen, $\mu mol\ kg^{-1}$	ALK, $\mu eq\ kg^{-1}$	DIC, $\mu mol\ kg^{-1}$	$\Omega_{C,bw}$,* %
2A	2322	128	2404	2345	91± 13
2B	2335	128	2404	2345	91± 13
3	2966	140	2411	2358	75± 11

*The uncertainty in $\Omega_{C,bw}$ is due to the uncertainty in calculating carbonate ion concentration from the alkalinity (ALK) and dissolved inorganic carbon (DIC) measurements and the uncertainty in the 1-atm calcite solubility product.

Setting

Three stations were occupied on the Ontong-Java Plateau, a topographic high in the western equatorial Pacific (Figure 1), on a cruise by the R/V *Moana Wave* in June of 1991. Two of the stations at ≈2300 m are spatially separated by less than 1 km, vertically by less than 15 m, and are considered duplicates.

The plateau has high calcite (>70% by dry mass) from 1500 m to nearly 5000 m, and is in a uniformly low productivity portion of the world's oceans [*Berger et al.*, 1987]. This location is ideally suited to address the stated goals because (1) the sediments are well characterized here, including estimates of dissolution from sedimentary indicators [e.g. *Berger et al.*, 1982] and rates of sediment accumulation and benthic mixing [*Berger and Killingley*, 1982], and (2) Jahnke *et al.* [1994] based their conclusions regarding metabolic dissolution on benthic flux chamber results from two sites here. One of these, the station referred to by Jahnke *et al.* as "NS", is the same as our station 3.

This study represents the first successful attempt to quantify the rate of calcite dissolution with both benthic chamber and in situ electrode measurements at the same site. The pertinent bottom water characteristics of the stations are summarized in Table 1. The range in estimated bottom water saturation state with respect to calcite is due to uncertainties in both the bottom water carbonate ion and the estimated solubility product for calcite.

Methods

In Situ Electrode Measurements

The microelectrode measurements were made in situ by an updated version of the profiler used by *Hales et al.* [1994], deployed on a free-vehicle lander. This a substantial improvement over the box-core deployment method followed by *Hales et al.* [1994] and *Archer et al.* [1989], because of decreased wire time and the decreased potential for introducing artifacts associated with taking a core. On each deployment, the profiler was configured with one resistivity, four oxygen, and four *p*H electrodes. All electrodes used were of the same type as used by *Hales et al.* [1994]. Electrode measurements were made at 0.25-0.5-cm vertical intervals from a few centimeters above the sediment-water interface to as much as 9 cm below. Each measurement is the average of the last five readings out of a suite of 15 readings made once every 10 s.

The vertical spacing between measurements is known very well; the location of the interface relative to each oxygen and *p*H electrode was determined from their respective profiles: Each profile included a series of measurements in the overlying water that showed little change as the depth increased. The first measurement that deviated significantly from these was assumed to be below the sediment-water interface, and the location of the interface was determined by interpolation (estimated accuracy is about 20% of the vertical interval or 0.5-1.0 mm). The interface for the resistivity electrode was determined by interpolation as the depth where the resistivity was 10% higher than it was in the bottom water [*Archer*, 1990]. The interface determined by measuring the length difference between the resistivity electrode and each of the others and assuming a flat seafloor was not systematically different from the above method.

Electrode drift was assessed by making two measurements of each electrode in the overlying water after the profile was completed. If these values differed from those in bottom water prior to entering the sediment by more than 10% (15% for resistivity) of the total change recorded by the electrode, that profile was discarded. Two of the four oxygen electrodes performed acceptably at each station. Two *p*H electrodes performed acceptably at station 2A, but only one performed acceptably at stations 2B and 3.

Oxygen electrodes were calibrated in situ by assuming a linear relation between the signal in bottom water (concentration determined by Winkler titration) and the open circuit reading (zero oxygen concentration). We have shown that the assumption of an open circuit reading at zero oxygen is valid with measurements in oxygen depleted sediments in Puget Sound (B. Hales, unpublished data, 1990). The *p*H electrodes were calibrated on the ship prior to deployment with *p*H 7 and *p*H 8 buffers, made up to the ionic strength of seawater with KCl. The difference between these solutions and seawater may mean there are different liquid junction potentials for the electrodes between the buffers and seawater. This is not a significant error, however, since we are interested in the *p*H differences between bottom water and pore water (ΔpH), not the absolute value of the seawater *p*H. The slope thus determined was corrected for the temperature difference between the laboratory and the bottom water using the Nernst equation. Error bars on each electrode measurement below the interface include the uncertainty due to both short-term variability (i.e., the standard deviation of the five readings of each electrode at each depth) and the uncertainty due

to the differences between the measurements in bottom water before and after profiling (i.e., "drift"). Most of the uncertainty derives from the latter.

Bulk Sediment Measurements on Retrieved Cores

Sediment samples were taken from subcores of Soutar box cores at two locations. One set of samples was taken at 2-3-mm resolution over the upper 10 cm of the sediment, and another was taken at ≈1 cm resolution over the upper 30 cm of the sediment. Both sets of samples were analyzed for particulate organic carbon and total carbon by a Carlo-Erba CHN analyzer. Organic carbon was measured on samples that had been treated with HCl vapor followed by direct additions of ultrapure HCl to each sample to remove all solid carbonates [*Hedges and Stern*, 1984]. Calcium carbonate content was calculated assuming the difference between acid-treated and untreated samples was entirely due to calcium carbonate. Porosity was calculated from measurement of the dry mass of the fine-resolution samples and the salt content of the samples.

Bottom Water Properties

Temperature and salinity were taken from the nearest Geochemical Ocean Sections Study (GEOSECS) station, at corresponding depths. Bottom water oxygen was determined on the ship by Winkler titration on bottle samples. Bottom water alkalinity (ALK) and dissolved inorganic carbon (DIC) were determined by Gran titration with ultrapure HCl in a closed cell monitored by a Ross *p*H electrode. The titration was calibrated with ALK and DIC standards (A. Dickson, Scripps Institution of Oceanography, personal communication, 1991). Precision of replicate alkalinity and DIC measurements was less than 0.25%. There was an artifact associated with the volume of the titration cell, which appeared to be systematically increasing in volume over the course of the cruise. As a result, samples titrated later in the cruise yielded estimates of ALK and DIC that were up to 1% higher than samples from the same locations titrated earlier. However, the most important parameter for this study was the carbonate ion concentration ($[CO_3^{2-}]$). The accuracy with which $[CO_3^{2-}]$ could be determined was relatively insensitive to this cell volume error, since it affected ALK and DIC similarly. There was no significant difference between $[CO_3^{2-}]$ determined from titrations performed earlier and later in the cruise. Calculation of $[CO_3^{2-}]$ is very sensitive to errors in ALK and DIC; the anlaytical precision of 0.25% in both measurements yields uncertainty in the calculated $[CO_3^{2-}]$ of about ±6%. Uncertainties in the dissociation constants of carbonic and boric acids [*UNESCO*, 1987] have less effect, since calculation of $[CO_3^{2-}]$ from ALK and DIC depends on the ratios of the constants and not the absolute values. Even given the uncertainty in calculation of $[CO_3^{2-}]$, these stations are more undersaturated with respect to calcite than similar depths at the nearest GEOSECS station, which is nearly 2000 km east of the Ontong-Java Plateau. This follows the general trend of a westward-shoaling of the calcite saturation horizon evident in the GEOSECS equatorial data.

Pore Water Models

The pore water O_2 and *p*H data were interpreted using one-dimensional, steady state mathematical models simulating diffusion and reactions in the sediment. Boundary conditions in all cases were bottom water concentrations at the interface and zero-derivatives at the deepest part of the model. Both models were solved by discretizing the differential equations describing the system and inverting the resulting matrices using a tridiagonal approach [*Press et al.*, 1989]. The oxygen model was linear and independent of the *p*H model, so it could be solved directly. Numerical solutions were verified by comparison to analytical solutions. The *p*H model required simultaneous solution of the distributions of ALK, DIC, and dissolved calcium, Ca^{2+}. Species included in ALK and/or DIC were CO_2^* ($CO_{2(aq)} + H_2CO_3$), HCO_3^-, CO_3^{2-}, and $B(OH)_4^-$. The species HCO_3^- and $B(OH)_4^-$ were eliminated algebraically from the equations, using the acid-base equilibrium relationships between them and the other species and the dissociation constants for carbonic and boric acids suggested by *UNESCO* [1987]. This left a combination of three coupled, nonlinear differential equations with CO_2^*, CO_3^{2-}, and Ca^{2+} as the dependent variables. Because of the nonlinearity, the tridiagonal inversion of the matrices defined by these discretized equations had to be executed iteratively, using Newton's method [*Press et al.*, 1989]. The pore water pH data are presented as ΔpH, the difference between pore water *p*H and bottom water *p*H. For comparison to the data, modeled pore water Δ*p*H was calculated from the resulting model solution for CO_3^{2-} and CO_2^* from the relationship

$$\Delta pH = 0.5 \log \left[\frac{\left[CO_2^*\right]_{BW}\left[CO_3^{2-}\right]_{PW}}{\left[CO_2^*\right]_{PW}\left[CO_3^{2-}\right]_{BW}} \right], \quad (3)$$

where the subscripts BW and PW distinguish concentrations in bottom water and pore water, respectively. This result is relatively insensitive to the choice of equilibrium constants for carbonic and boric acids, as long as a consistent buffer system is employed. Diffusivity in the pore waters is approximated by $D_{i,PW} = D_i/F$ [*Berner*, 1980; *McDuff and Ellis*, 1979] where D_i is the diffusion coefficient for species *i* in "clear" water and F is the sediment formation factor, determined by measurements with the resistivity electrode. Diffusion coefficients were taken from *Li and Gregory* [1974] (for Ca^{2+}, HCO_3^- and CO_3^{2-}); *Broecker and Peng* [1974] (for CO_2^*); and *Wise and Houghton* [1966] (for O_2). Borate ion ($B(OH)_4^-$) was assumed to have the same diffusion coefficient as HCO_3^-. The models included a diffusive sublayer that was 0.5 mm thick; diffusivities in this layer were assumed to equal the clear water diffusivities; respiration and dissolution rates were zero in the diffusive sublayer.

Results

Bulk sediment properties for the top 10 cm of the sediments are presented in Figure 2. Calcite contents are fairly constant with depth at 85-92%. There is slightly higher calcite at station 2 than at station 3, but the difference is similar to the reproducibility of each measurement (based on duplicate measurements of the same sample). Organic carbon is consistently low (0.1-0.4%) at both stations, with station 3 being slightly enriched over station 2. The organic carbon content at both stations decreases weakly over the top 10 cm, but the change is small relative to the measurement error, and the decrease is not by any means continuous. For this reason the organic carbon data were not used to constrain the rates of respiration within, or the flux of metabolizable carbon to, the sediment.

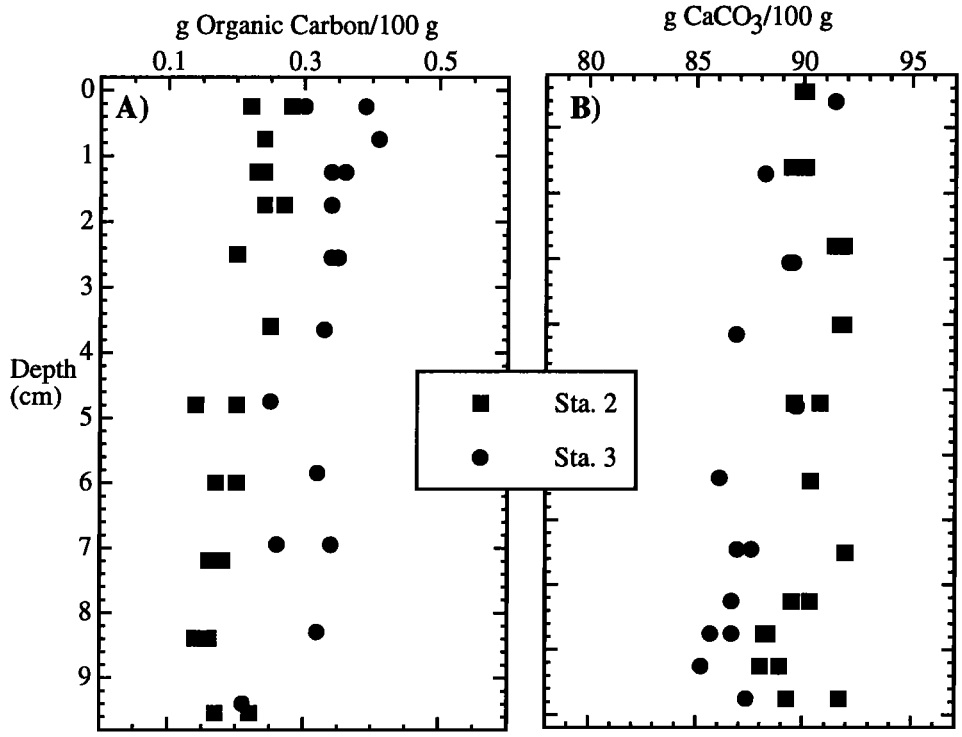

Figure 2. Solid carbon content of Ontong-Java Plateau sediment, as percentages of the total solids: (a) organic carbon and (b) calcium carbonate.

The microelectrode data are shown in Figure 3. The formation factor (Figure 3a), defined as the ratio of resistivity in the sediments to that in the overlying water, reaches a fairly constant value of about 2 by 3-4 cm below the interface at all stations. Porosity ϕ is related to formation factor F by the relationship

$$\phi = F^{-\frac{1}{b}} \tag{4}$$

[*Andrews and Bennett,* 1981]; porosity measured on subsamples from box cores decreased to constant values of about 70% by 3-4 cm below the interface (data not shown), implying that the exponent b is about 2. Oxygen (Figure 3b) decreases smoothly throughout the measurement region, showing curvature even at the deepest penetration of the electrodes. The *p*H data is presented as ΔpH, the difference between pore water *p*H and bottom water *p*H (Figure 3c). Negative values of ΔpH mean that the pore water is more acidic than the bottom water; positive values indicate the opposite. All electrodes at all stations show a shift toward lower *p*H below the interface to a minimum, and a gradual return towards (in one case even beyond) bottom water values. There are several interesting qualitative features of these data. The first is the significant difference between the two sets of oxygen profiles at Stas. 2A and 2B, implying differences in the oxygen flux into the sediments between these two stations.

The *p*H profiles are also different between the two stations, with the *p*H minimum at station 2B being roughly twice as low as at station 2A. Since the saturation state of calcite must be similar at the two sites, the more acidic pore waters at station B must be due to the greater respiration rates in the sediments, as implied by the oxygen gradients. Also remarkable is the existence of minima in the *p*H profiles and the return toward, and even beyond (at station 2A), their bottom water values at depths >2 cm below the interface. This could not happen without dissolution of some carbonate mineral at depths of a few centimeters in the sediment. These stations are strongly undersaturated with respect to aragonite in the bottom waters, and it is unlikely that a significant amount of this mineral could persist to these depths [e.g. *Hales et al.,* 1994]. Indeed, *Berger et al.,* [1982] observed no aragonite in the sediments they collected from the Ontong-Java Plateau at these depths. The only conclusion that can be drawn is that calcite is actively dissolving within the sediments.

Discussion

We interpreted the pore water data by simulating the vertical distributions of oxygen and *p*H with steady state, one-dimensional diffusion and reaction models to evaluate the pertinent reaction rates in the sediment. The approach is essentially the same as used by *Hales et al.* [1994], and the governing equations and numerical solutions are described in detail by *Hales* [1995].

The Pore Water O_2 Model

Pore water oxygen simulations are sensitive to the depth-dependent rate of oxygen consumption $R_{O2}(z)$ assumed to follow the empirical form:

$$R_{O2}(z) = (1-\phi)\left(r_1 e^{-r_2 z} + r_3 e^{-r_4 z}\right); \tag{5}$$

where ϕ is the porosity (calculated from the formation factor data

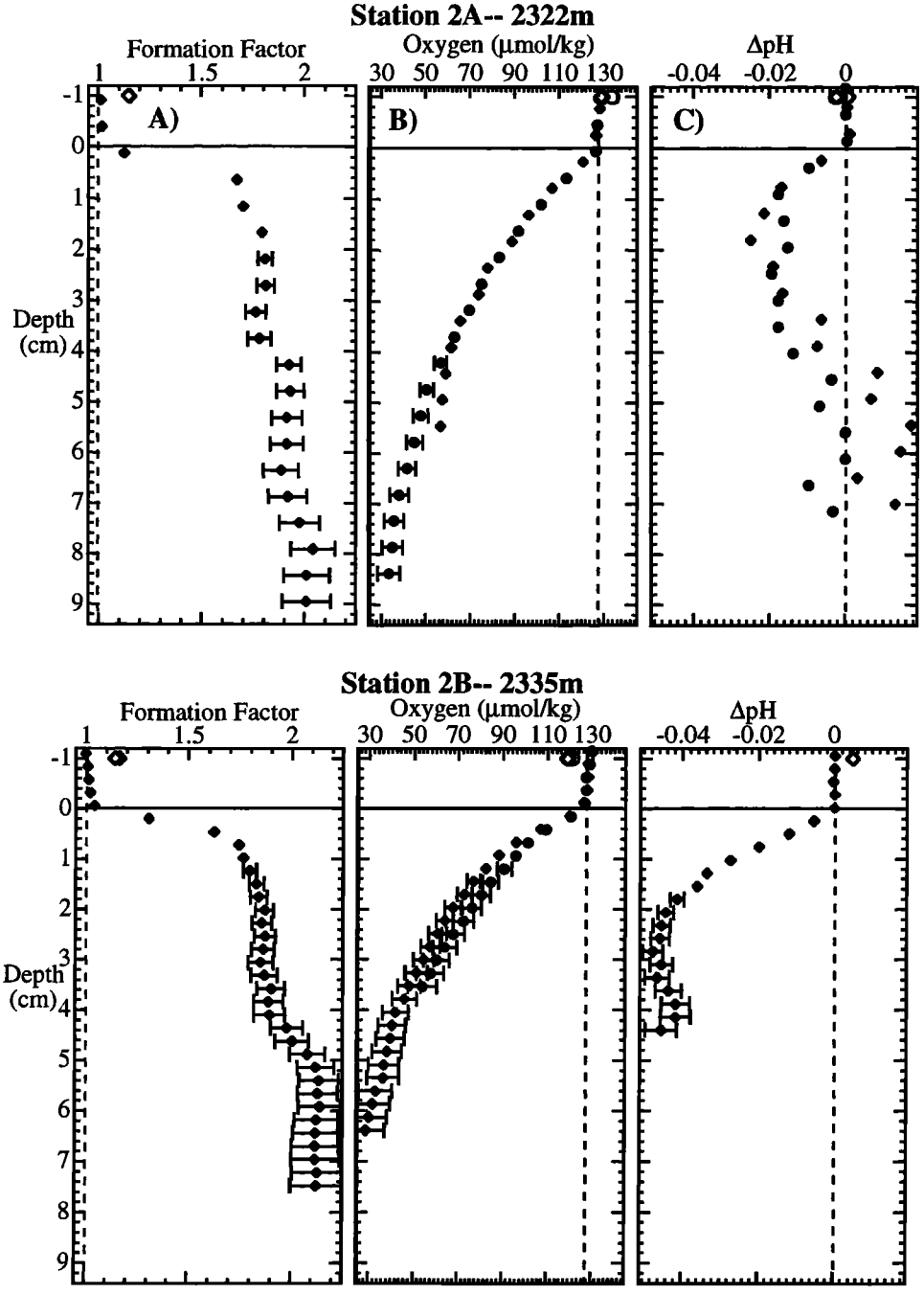

Figure 3. In situ electrode data from the Ontong-Java Plateau: (a) formation factor, defined as the ratio of the resistivity measured in the sediment to that measured in the overlying water, (b) porewater oxygen, and (c) porewater *p*H, expressed as ΔpH, the difference between porewater *p*H and bottom water *p*H. In figures 3a-3c, depth is expressed positive downward, with the sediment-water interface at zero (solid horizontal line). The vertical dashed lines represent the bottom water value of each property. Different shaped symbols in the same plot represent measurements made by separate electrodes. Profiles represented by the diamonds will be referred to as profile 1, those represented by the circles will be referred to as profile 2. In all plots, the larger, open symbols 1 cm above the interface are measurements made after completing the sediment measurements, represented by the smaller solid symbol of the same shape. In some cases, these points are partially obscured by the measurements prior to penetration of the sediment. All measurements below the sediment water interface have error bars; those not visible are smaller than the symbols themselves. Since the measurements above the interface are all replicate measurements of bottom water, their scatter is indicative of their reproducibility and error bars are not given.

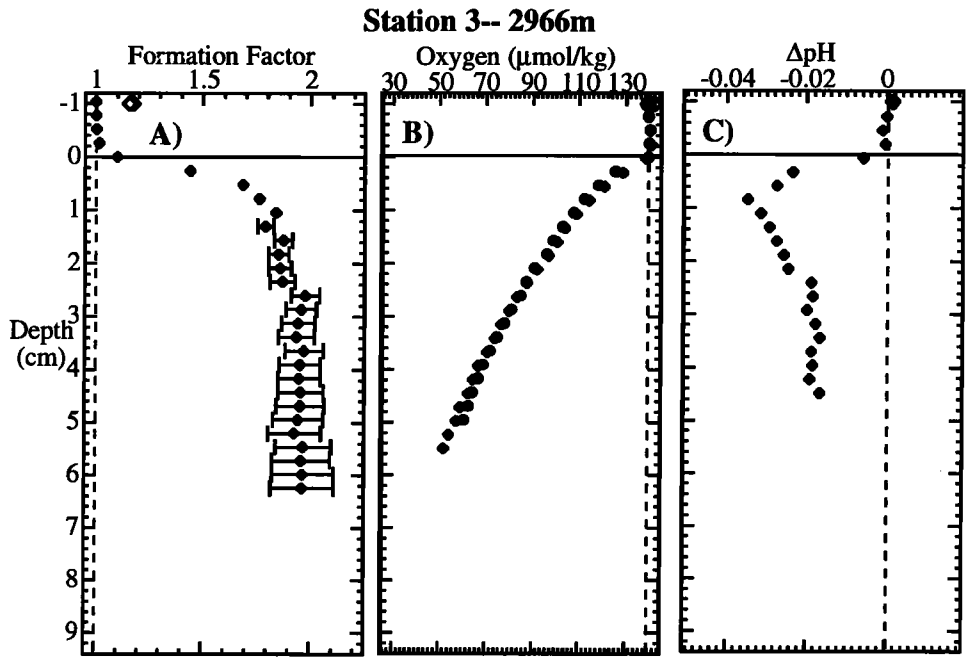

Figure 3. (continued)

and (4)) and r_1, r_2, r_3, and r_4 are adjustable parameters. This expression of R_{O2} is similar to that used by *Hammond et al.*, [1996] and is slightly more detailed than that used by *Hales et al.*, [1994], who used at most three adjustable parameters, and did not explicitly include the dependence on the solid fraction of the sediments, (1- ϕ). Although conceptually similar to a "multi-G" model of organic carbon degradation [*Berner*, 1980], our goal was only to match the oxygen profile as accurately as possible. Determination of the optimum combination of four adjustable parameters manually is difficult, so the oxygen model was executed by an optimization routine (Powell's method, *Press et al.*, 1989] that adjusted r_1, r_2, r_3, and r_4 to minimize the deviation between the data and the model output.

Figure 4 illustrates the need for inclusion of all four adjustable rate parameters (two exponential terms) in order for the model to fit the oxygen data throughout the profile; results for other cases are summarized in Table 2, where there are some trends worth noting. In all simulations, most (≥70%) of the oxygen consumption is due to the first exponential term in (5), which has a scale depth ($1/r_2$) of 1.7-3.5 mm. This means that most of the CO_2 was generated very near the interface. As expected, oxygen fluxes calculated from the model output at station 2B are greater than those at station 2A. This difference is greater than the difference between individual profiles at each station, but is only

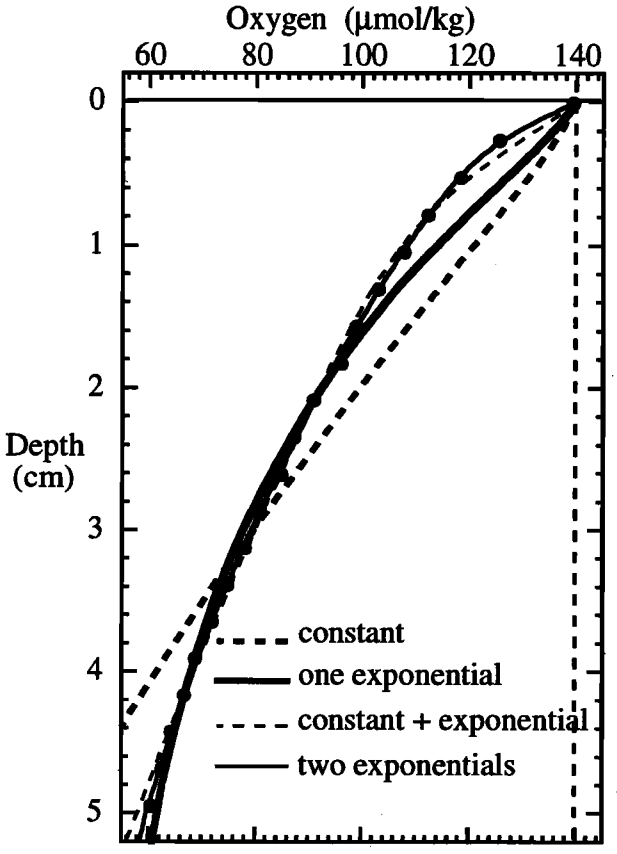

Figure 4. Example oxygen model output for station 3, compared to oxygen profile 2. Model output with respiration rates that are constant with depth (heavy dashed line); a single, exponentially decaying function of depth (heavy solid line); or a combination of a constant and a single exponential (light dashed line) do not provide adequate agreement with the data over the entire depth range, while that with a two-exponential formulation does (light solid line). The inflection near the interface in the profile with respiration described by a single exponential (heavy solid line) is due to the fact that the gradient in formation factor is significant relative to the reaction term in that depth interval. Note that each exponential term contains two empirical parameters (see, e.g. (5)).

Table 2. Oxygen Model Results

		Oxygen Consumption Rate Parameters*				
Station	Profile	r_1, μmol O_2 $(cm^3$ sed. solids$)^{-1}$ yr^{-1}	r_2, cm^{-1}	r_3, μmol O_2 $(cm^3$ sed. solids$)^{-1}$ yr^{-1}	r_4, cm^{-1}	Integrated (Net) Consumption, μmol O_2 cm^{-2} yr^{-1}
2A	1	111	2.85	8.50	0.352	9.7
	2	192	4.25	6.57	0.277	9.6
2B	1	262	2.87	6.86	0.318	18.7
	2	305	3.47	2.69	0.132	16.8
3	1	281	4.18	3.09	0.200	14.0
	2	854	6.17	3.45	0.228	21.1

*The rate parameters r_1, r_2, r_3, and r_4 from (5) are determined by an optimization routine as the combination that minimizes the deviation between the model simulation and the porewater oxygen data [see *Hales*, 1995]. The integrated consumption is calculated from this best-fit simulation and is opposite and equal to the flux at the sediment-water interface.

slightly greater than the difference between the two estimates at station 3, implying that the variability in benthic oxygen flux is as large over spatial scales of a few centimeters as it is over a few thousand meters. The two estimates of oxygen flux to the sediment at station 3, 14 and 21 μmol cm^{-2} yr^{-1}, are in good agreement with the flux predicted by the benthic chamber measurements, 18±8 μmol cm^{-2} yr^{-1}.

Considering the detailed sensitivity analysis of the *p*H model that follows, some discussion of the uncertainties associated with the r_i parameters of (5) is justified. There are, of course, uncertainties in these parameters for a given oxygen profile that are not shown in Table 2. Because of the shallow scale depth of the first exponential term in (5), (even when the increase in the term $(1-\phi)$ is considered, the scale depth of this term is of the order of 2.5-5 mm), the parameters r_1 and r_2 are the least tightly constrained, and we will limit the rest of this discussion to those terms. Constraint of these values is difficult to address unequivocally, because they are so dependent on one another. If, for example, r_1 is held constant, adjustments of only a few percent in r_2 generate model profiles that do not approximate the data acceptably; the same is true if r_2 is held constant and r_1 varied. However, if both are allowed to vary in such a way that the implied O_2 flux to the sediment remains within a few percent of the optimum, r_1 and r_2 values as much as 20% different from the optima in Table 2 yield acceptable approximations of the electrode data. These uncertainties, however, are smaller than the differences implied by inter-electrode variability. In the following section, uncertainties in R_{O2} will be limited to only the different sets of r_is implied by the different electrodes. In that way, R_{O2} is treated as a single input parameter to the *p*H model, rather than four, with limits that are defined by the optimum fits to the two observed O_2 profiles at each station.

The Pore Water *p*H Model

Model simulations of pore water *p*H are sensitive to two reactions, the dissolution rate of calcite ($R_{d,C}$, as expressed by (1)) and the rate of CO_2 production during metabolism of organic carbon R_{CO2}. Uncertainties in the magnitude and depth dependences of these reactions must be addressed before attempting to quantify the calcite dissolution implied by the *p*H data.

Assuming that the order of the dissolution reaction n_C is known to equal 4.5, the important parameters controlling the calcite dissolution rate are the dissolution rate constant $k_{d,C}$ and the saturation state of the bottom water with respect to calcite $\Omega_{C,bw}$. The rate constant has a wide range of reported values. *Keir* [1980] determined that $k_{d,C}$ was over 1000% d^{-1} with laboratory measurements of the dissolution rate of natural sediments, while *Jahnke et al.* [1994] reported a range of 0.05-0.5% d^{-1}, based on in situ measurements of seafloor calcium and alkalinity fluxes. This is a relative difference of over 10^4, leaving essentially no predetermined limits on this parameter. We examined rate constants in the range 10^{-3}-10^4% d^{-1}, which includes all previous estimates. The bottom water saturation state depends on both the thermodynamic solubility product $K_{sp,C}$ and the bottom water carbonate and calcium ion concentrations. The uncertainties in the measured bottom water DIC and ALK lead to uncertainties in the calculated carbonate ion concentration of up to 6%. The *UNESCO* [1987] solubility product is about 8% higher than the lower limit of estimates based on *Mucci's* [1983] 1-atm solubility and similarly lower than the upper limit of those based on *Plath et al.*'s [1980] 1-atm solubility measurements. This means that our estimate of $\Omega_{C,bw}$ has uncertainties of about ±14%, which we used to define the practical limits. This assumes that *Millero's* [1983] pressure dependence is correct; at these depths, the pressure dependence of *Ingle* [1975] predicts only about a percent higher solubility.

Metabolic CO_2 production is linearly proportional to the rate of oxygen consumption:

$$R_{CO2} = \beta R_{O2}, \tag{6}$$

where ß is a stoichiometric constant. At each station there are two estimates of R_{O2}, determined by the two oxygen profiles at each station (see Table 2). As stated previously, the differences

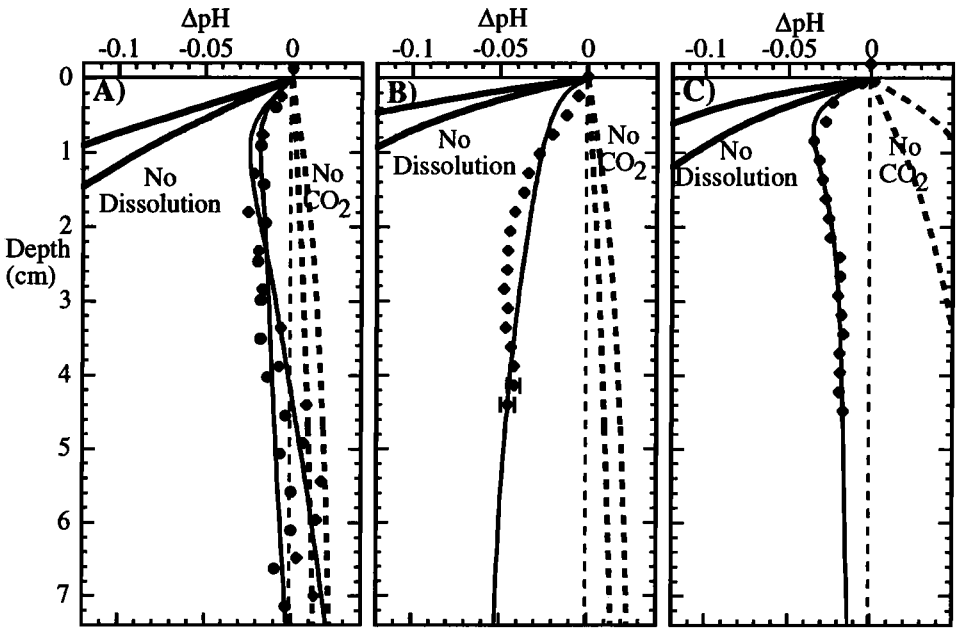

Figure 5. Model *p*H curves at (a) station 2A, (b) station 2B, and (c) station 3, for three scenarios: no dissolution (heavy solid lines), no metabolic CO_2 production (heavy dashed lines), and the best fit to the data (light solid line).

between these two estimates of R_{O2} are greater than uncertainties in each estimate, and the practical limits on this parameter are defined by the two estimates. The constant ß can be between 0.55 (alkane equivalent organic carbon; see *Hales et al.* [1994] or 0.77 (Redfield organic carbon). A recent water column study [*Anderson and Sarmiento,* 1994] estimated this parameter to be 0.69, and a benthic flux chamber experiment [*Hammond et al.,* 1996] gave an estimate of 0.67, but the reported error bars were large enough that these estimates did little to discriminate between the upper and lower limits stated above. We used the above range (0.55 to 0.77) as the practical limits on ß.

The primary goal of the *p*H modeling exercise was to assess the importance of calcite dissolution driven by metabolic processes relative to that driven by bottom water undersaturation. As a first step, we addressed two simple cases that included no metabolic dissolution of calcite. These are (1) the "no dissolution" case, where the respiration reaction produces carbonic acid, but no calcium carbonate dissolves (effectively the same as assuming that $k_{d,C}$ is zero), and (2) the "no CO_2" case, where the respiration reaction does not produce carbonic acid while consuming oxygen (effectively the same as assuming that ß is zero), and calcite dissolves only in response to bottom water undersaturation. The range in *p*H for these two cases is presented in Figure 5, along with a scenario including metabolic dissolution that provides the best fit to the *p*H data in the range of input parameters investigated (described below). The two no dissolution curves represent the range of possible solutions given the two different estimates of the oxygen consumption rate at each station and the practical range of ß; the two no CO_2 curves represent the range of solutions for the saturation state of the bottom waters given in Table 1 and dissolution rate constants of 0.05% and 0.5% d^{-1} (the range suggested by *Jahnke et al.* [1994]). It is worth noting that no combination of dissolution parameters in the no CO_2 case can generate negative values of Δ*p*H, in contrast to all the observations. Furthermore, the no dissolution simulations greatly overpredict the acidification of the pore waters. It is clear that neither case excluding the effects of metabolic dissolution can reproduce the observations, and that dissolution driven by metabolic CO_2 production must play a significant role in determining the pore water chemistry at these stations.

To address the apparent disagreement between the *p*H data and the no metabolic dissolution scenarios, we determined the constraints posed by the *p*H data on the dissolution flux predicted by the model, given the practical limits on the four model inputs discussed above. Figure 6 demonstrates the sensitivity of the model simulations to these parameters. Sensitivity to ß (Figure 6a) over its entire practical range is similar to a factor of 2 adjustment in the rate constant (Figure 6b). The most sensitivity, however, is to the bottom water saturation state. A similar shift in model *p*H results if this value is altered only about a percent from its optimum value. This sensitivity to $\Omega_{C,bw}$ means that, in some cases, the *p*H data themselves provide a better constraint on this parameter than the bottom water measurements of alkalinity and DIC.

The first step in constraining the model simulations was choosing a statistic that quantified the deviation between model simulations and the data. We chose the "average relative absolute deviation" (ARAD), defined by:

$$\mathrm{ARAD} \equiv \frac{1}{N}\sum_{i=1}^{N}\frac{|m_i - d_i|}{\sigma_i}, \tag{7}$$

where N is the number of data points in a given profile, m_i is the model output at depth i, d_i is the value of the data at that point, and σ_i is the analytical standard deviation of the data at that point, as described in the methods section. The ARAD is a linear version of the familiar χ^2 which is then averaged over the number

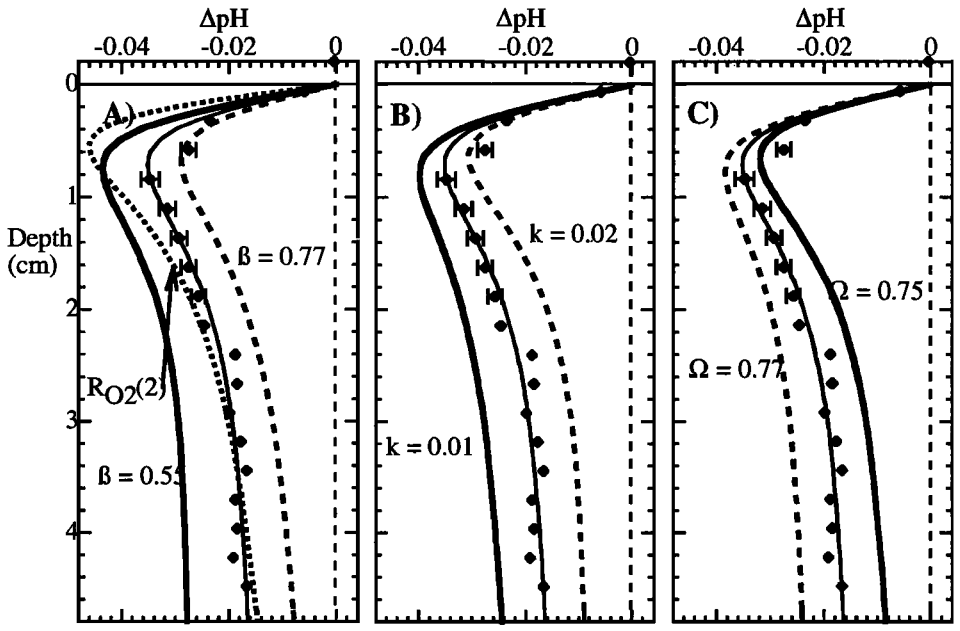

Figure 6. Demonstration of the sensitivity of the *p*H model output at station 3 to (a) the depth-dependent rate of CO_2 generation, (b) dissolution rate constant, and (c) bottom water saturation. In all cases, the light solid line is the model output with $k_{d,C}$ = 0.014% d^{-1}, $\Omega_{C,bw}$ = 76%, ß = 0.64, and the oxygen consumption rate determined by oxygen profile 1. The other curves in figures 6a-6c are the same as this curve, with one of these parameters altered. In Figure 6a, the heavy solid line is the result if ß is 0.77; the heavy dashed line has ß = 0.55. The heavy dotted line is output if the oxygen consumption rate determined by oxygen profile 2 is used. Figure 6B shows the result if $k_{d,C}$ = 0.01% d^{-1} (heavy solid line) or 0.02% d^{-1} (heavy dashed line). Figure 6C shows the output for $\Omega_{C,bw}$ = 75% (heavy dashed line) and $\Omega_{C,bw}$ = 77% (heavy solid line).

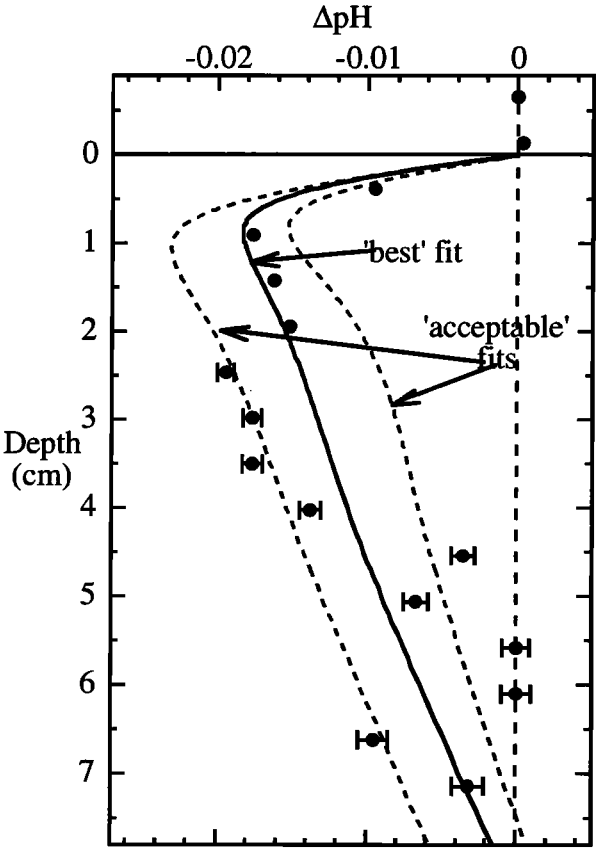

of data points in the profile. It is a more 'robust' statistic than higher-order statistics like the χ^2, because the dependence on $|m_i-d_i|$ is less sensitive to outlying points than higher-order terms like $(m_i-d_i)^2$ [*Press et al.*, 1989]. (This statistic is the one minimized in the oxygen rate determination described above.) The second step was to search the range of input parameters until we found a minimum value of the ARAD. Because every data profile has different analytical error bars and different degrees of "noisiness", there was no universally acceptable value of this statistic for all profiles, and we visually evaluated the model output to assess the "goodness" of fit. This is precisely what *Press et al.* [1989] refer to as "chi-by eye", but the presence of variability in the observations that we cannot expect the model to reproduce within the analytical uncertainties of the measurements (e.g., the variability in the *p*H data at station 2A below 4 cm) left us with no other alternative.

The minimum ARAD, or "best fit" case was evaluated for each *p*H profile to decide whether or not the fit was good enough

Figure 7. Example *p*H model profiles defining the "region of agreement" with the data. The solid line is the model solution with the lowest ARAD, or best fit. The two dashed lines are model simulations that fit the data acceptably; simulations that fit worse than these dashed lines have greater ARAD statistics and are deemed unacceptable reproductions of the data. Data shown here are *p*H profile 2 from station 2A; this procedure was repeated for *p*H profile 1 at this station and the profile at station 3.

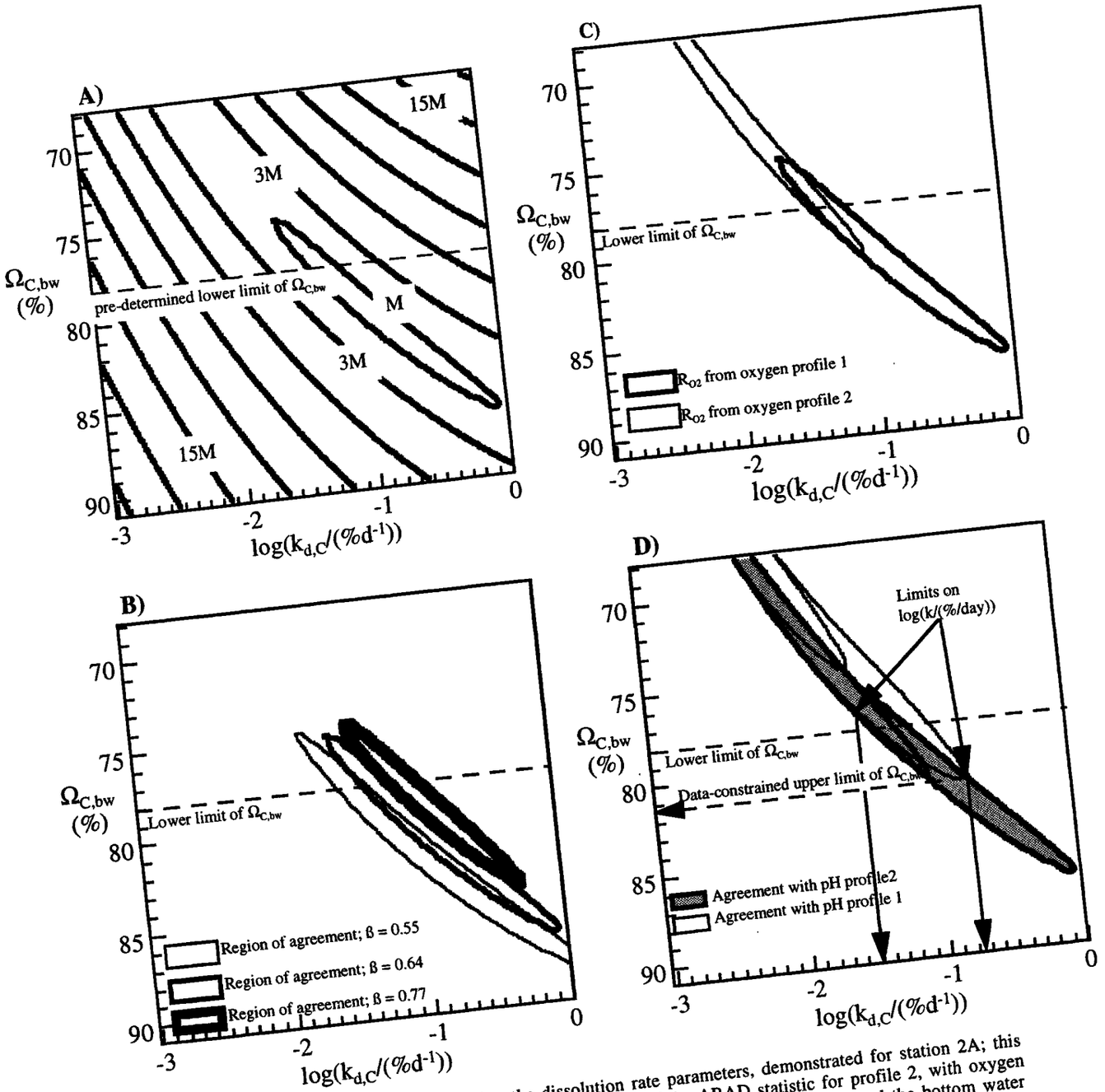

Figure 8. The procedure for constraining the dissolution rate parameters, demonstrated for station 2A; this procedure was also followed for station 3. (a) Contour plot of the ARAD statistic for profile 2, with oxygen consumption rate 1, ß = 0.64, as a function of the log of the dissolution rate constant and the bottom water saturation state. The contour labeled "M" denotes the maximum allowable value of the ARAD and corresponds to combinations of $k_{d,C}$ and $\Omega_{C,bw}$ yielding solutions that fit the data as well as the dashed lines in Figure 7. Solutions within the contour fit the data better than the dashed lines; solutions outside fit worse. The other contours represent multiples of the maximum allowable value of ARAD; that is, contours labeled 3M represent model solutions that deviate from the *p*H data by a factor of three more than the dashed lines in Figure 7. For clarity, Figures 8b-8d will show only the region of acceptable fit (ARAD ≤ M). (b) The sensitivity of the region of acceptable fit to changes in stoichiometry of the respiration reaction ß. For clarity, only the contours with ß = 0.64 will be shown in the Figures 8c and 8d. (c) Regions of acceptable fit to *p*H profile 2 for oxygen consumption rates determined by oxygen profiles 1 and 2, ß = 0.64. Since there is no way of knowing which respiration rate is more appropriate for pH profile 2, the region of agreement for both cases must be considered. (d) Same as Figure 8c, but with region of agreement with *p*H profile 1 superimposed. No value of $\Omega_{C,bw}$, greater than 81% is compatible with *p*H profile 1; since both profiles must have the same value of $\Omega_{C,bw}$, the maximum value of $\log(k_{d,C}/(\text{percent per day}))$ for this case (ß = 0.64) is -0.8. Given the predetermined lower limit of $\Omega_{C,bw}$ = 78% for this station, the minimum value of $\log(k_{d,C}/(\text{ percent per day}))$ is -1.4. The same procedure for the limits of the respiration parameter ß gives the final limits on the dissolution rate parameters.

to merit discrimination of other model simulations against it. The model curves in Figure 5 show that, while not perfect, the best fit solutions for the two profiles at station 2A and the profile at station 3 did a good job of describing most of the variation in the data, while the best fit at station 2B did not do nearly as well. We will limit the rest of the analysis to Stas. 2A and 3. Given this "optimum" combination of parameters for each profile, we then adjusted the input parameters away from that optimum until the simulation no longer agreed with the given profile (Figure 7). The value of ARAD corresponding to these simulations was deemed the maximum allowable deviation from the data. Simulations with ARAD less than or equal this value fit the data better than the dashed lines in Figure 7 and were accepted as reasonable approximations of the data; those with greater ARAD values fell outside the dashed lines in Figure 7 and were not accepted as reasonable simulations.

The ARAD was tabulated as a function of the model input parameters and plotted in parameter space for each *p*H profile. Figure 8a demonstrates how the ARAD varies as a function of $k_{d,C}$ and $\Omega_{C,bw}$. The closed contour, labeled "M," represents the boundary of the "field of acceptable fit" to *p*H profile 2 at station 2A, driven by the respiration rate determined by oxygen profile 2 (at that station), with a stoichiometry of 0.64, as a function of $\log(k_{d,C}$ /(percent per day)) and $\Omega_{C,bw}$ (percent). Any combination of $k_{d,C}$ and $\Omega_{C,bw}$ within this contour gives an acceptable fit to the electrode data (see Figure 7); combinations outside the contour generate model simulations that deviate unacceptably from the observations. The fact that the field of acceptable fit has finite dimensions in $k_{d,C}$ and $\Omega_{C,bw}$ implies that the *p*H data is capable of constraining both of these parameters more tightly than the predetermined limits discussed above.

Figures 8b and 8c illustrate how the field of acceptable fit moves in this 'k-Ω space' in response to changes in R_{CO2}. Figure 8b demonstrates the effect of variable ß. (For the sake of clarity, this response will not be shown in Figures 8c and 8d.) The dependence on R_{O2} is shown in Figure 8c. Note that both estimates of R_{O2} and the entire practical range of ß generate model simulations that agree acceptably with the data within the practical limits of both $k_{d,C}$ and $\Omega_{C,bw}$. This means that, unlike the dissolution rate parameters, constraints on the respiration rate parameters ß and R_{O2} are not improved over the a priori limits stated above. An additional problem is that we do not know which rate of respiration was more appropriate for this *p*H profile; therefore we had to use the union (rather than the intersection) of the two fields corresponding to the two estimates of R_{O2} as the region of acceptable fit. A consequence of this is that additional estimates of R_{O2} can potentially expand the region of acceptable fit, and loosen the constraint a given *p*H profile has on the dissolution parameters.

Adding a second *p*H profile does provide further constraint on the field of acceptable fit in k-Ω space (Figure 8d), as the two profiles must have the same value of bottom water saturation. While it is not clear that they must necessarily have the same value of $k_{d,C}$ (e.g., because of spatial heterogeneity in the size distribution, surface area, or mass fraction of the calcite), the requirement of equal $\Omega_{C,bw}$ provided some further constraint on the value of $k_{d,C}$ (Figure 8d). Taking into account the uncertainties in R_{CO2}, the dissolution rate constant at this station must be between 0.025% and 0.16% d^{-1} (Table 3), and the bottom water saturation ratio with respect to calcite must be between the practical lower limit of 78% (determined previously, see Table 1), and a maximum constrained by the data of 81%.

Including the uncertainty in $\Omega_{C,bw}$ caused by uncertainty in the carbonate ion concentration, this upper limit implies that the solubility product at station 2A must be at least 5% greater than the *UNESCO* [1987] value, which is about equal to the stated uncertainties. It is, however, incompatible with the lower solubility suggested by Mucci [1983], which implies that the bottom water saturation state can be no lower than 85%. The upper limit of $\Omega_{C,bw}$ at station 2A also provides a more restrictive upper limit of $\Omega_{C,bw}$ at station 3, because the calcite solubility product ($K_{sp,C}$) at station 3 must be 11% higher than at station 2A, because of the difference in depth between the two stations. Following the above procedure, this additional constraint at station 3 restricts the value of $k_{d,C}$ to 0.005-0.05% d^{-1} there (Table 3). The inclusive range for both stations, 0.005-0.16% d^{-1} is at least 4 orders of magnitude lower than the values Keir [1980] determined from laboratory rate measurements. It is also lower than any other value previously determined in the field but follows the general trend of lower rate constants observed in field experiments than in the laboratory [*Archer et al.*, 1989; *Cai et al.*, 1995; *Hales et al.*, 1994; *Berelson et al.*, 1994; *Jahnke et al.*, 1994; *Martin and Sayles*, 1996].

Using the constraints of the *p*H profiles on these controlling parameters, we quantified the calcite dissolution fluxes. The total dissolution was plotted in parameter space and presented as contours, much as the ARAD. Simply superimposing the field of acceptable fit as determined above over these contours gave the range of dissolution flux constrained by the data. This procedure is illustrated in Figure 9 for station 2A, ß = 0.55 and 0.77, and oxygen consumption rate 1 from Table 2.

Note that the field of acceptable fit is essentially parallel to the flux contours in Figure 9 for a given value of ß. This means that the uncertainty in dissolution flux is relatively insensitive to

Table 3. The *p*H Model Results

Station	$k_{d,C}$, % d^{-1}	$\Omega_{C,bw}$, %	Total Dissolution, µmol cm^{-2} yr^{-1}
2A	0.025 - 0.16	78 - 81	3.5 - 6
3	0.005 - 0.06	68 - 80	3.5 - 6

The ranges in all of these quantities include uncertainties related to ß and R_{O2}. The lower limit of $\Omega_{C,bw}$ at station 2A is the predetermined limit based on the precision of the measurement of the alkalinity and dissolved inorganic carbon and the uncertainty in the solubility product. The pH observations constrain the upper limit at stations 2A and 3, and the lower limit at station 3.

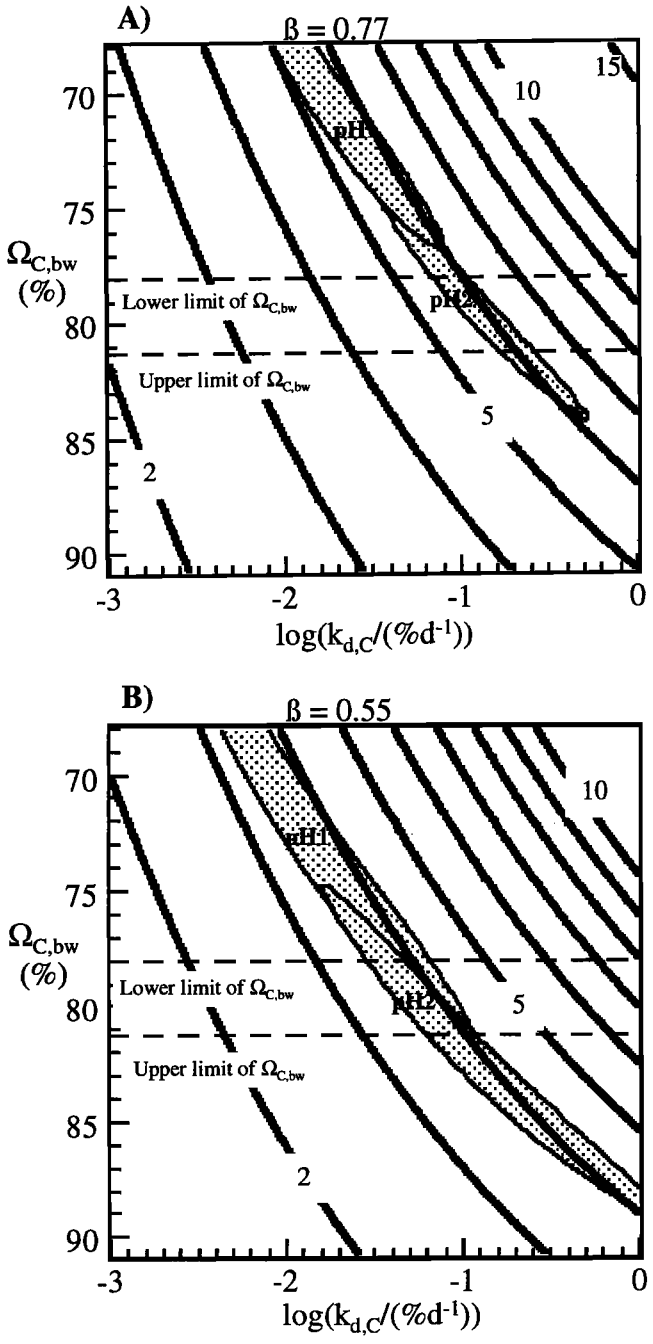

Figure 9. Example of dissolution flux estimation at station 2A for the oxygen consumption rate determined by oxygen profile 1, with ß equal (a) 0.77, and (b) 0.55. The heavy, labeled contours are calcite dissolution fluxes, with units of μmol cm^{-2} yr^{-1}. The regions labeled "pH1" and "pH2" are the limits of acceptable fit to the *p*H data determined previously. The allowable range in dissolution flux is constrained by these two regions and the limits placed on $\Omega_{C,bw}$ by the procedure described in the Figure 8 caption.

the above uncertainties in $k_{d,C}$ and $\Omega_{C,bw}$, in this field of k-Ω space. As a result, most of the uncertainty in the implied dissolution flux comes from the uncertainty in ß. Repeating this exercise for both stations and taking into account the ranges in the estimates of ß and R_{O2}, yielded the estimates of dissolution summarized in Table 3. Calcite dissolution fluxes at both stations are 3.5-6 μmol cm^{-2} yr^{-1}. Because a 40% increase in ß (from 0.55 to 0.77) gives a 70% increase in dissolution flux, there appears to be a superlinear dependence on ß, which is probably due to the high-order dissolution kinetics. The fact that the dissolution fluxes at stations 2A and 3 are similar despite the differences in total oxygen flux and bottom water saturation state is due to the shallower scale depths of the respiration reactions at station 3, and the lower range of $k_{d,C}$ constrained by the *p*H data there.

The predicted rate of calcite dissolution corresponds to 20-40% of the calcite rain to these sediments, given the sediment calcite content and independent estimates of the sedimentation rate [*Berger and Killingley,* 1982]. This is probably a lower bound of the fraction of the rain that is dissolved. For example, if a 1:1 ratio is assumed between the organic carbon and calcite fluxes to the sediment, then our estimates of dissolution correspond to 37-64% of the rain. In either case, dissolution accounts for a significant fraction of the rain to the sediments. Model runs with the same range of bottom-water saturation states and dissolution rate constants as in Table 3, but without metabolic CO_2 production (i.e., ß = 0) predict only about 1.2 μmol cm^{-2} yr^{-1} of calcite dissolution, implying that metabolic dissolution is responsible for 65-80% of the total.

Conclusions

We find that there is significant calcite dissolution in the sediments of the Ontong-Java Plateau and that the dissolution is driven primarily by metabolic CO_2. *Jahnke et al.* [1994] concluded from benthic flux chamber experiments at station 3 that dissolution driven by metabolic CO_2 was not as important as previous models had predicted. Fluxes predicted by both methods are summarized in Table 4. As noted previously, electrode-based oxygen fluxes are within the method errors of the fluxes determined by the benthic chamber measurement. Somewhat surprising is the fact that the range of calcium and alkalinity fluxes predicted from the models of pore water *p*H in this study overlaps with those reported by the benthic chamber technique. The reason for the apparent difference in the conclusions about the importance of metabolic dissolution between this work and that of Jahnke et al. is due to different representations of the respiration kinetics in the two studies.

Jahnke et al. [1994] simulated concentration changes in the chamber as a function of time using a sediment/pore water model that approximated respiration as a reaction that was first-order with respect to organic carbon, following the work of *Archer et al.* [1989] and *Archer and Maier-Reimer* [1994]. This gave a respiration rate that varied with depth in the sediment by means of a single exponential term. Given the stated bioturbation coefficient and respiration rate constant, the scale depth for the respiration reaction in *Jahnke et al.*'s [1994] model was about 1.5 cm. In contrast, the pore water oxygen profiles measured by the electrodes required two exponential terms to fit the data. Most (≥70%) of the oxygen consumption was accounted for by the term with scale depths of 0.2-0.4 cm. Thus more of the metabolic CO_2 production was shifted toward the sediment-water interface where it had a greater chance of diffusing out of the sediments before it could promote dissolution. We ran several model simulations comparing the dissolution flux driven by the two-exponential model of respiration to that driven by a first-order

Table 4. Comparison to Benthic Chamber Results at Station 3

Method	Flux		
	Oxygen, $\mu mol\ cm^{-2}\ yr^{-1}$	Calcium, $\mu mol\ cm^{-2}\ yr^{-1}$	Alkalinity, $\mu mol\ cm^{-2}\ yr^{-1}$
Benthic chamber *[Jahnke et al., 1994]*	-18±8	0.35±4.2	1.4±6.3
Pore water profiles (this study)	-14 - -21	3.5 - 6	5.5 - 10

Negative signs on the oxygen fluxes indicate that the flux is to the sediment, while the fluxes of calcium and alkalinity are out of the sediment. Calcium fluxes based on the porewater electrode measurements are equal to the total dissolution (Table 3). Alkalinity fluxes are calculated from

$$F_A = 2F_{Ca} + 0.15\beta F_{O_2}$$

where F_A, F_{Ca}, and F_{O2} are the alkalinity, calcium, and oxygen fluxes, respectively, and 0.15ß is the stoichiometric relationship between oxygen consumption and nitrate production, assuming Redfield C:N stoichiometry.

model. For all other parameters equal, the first-order respiration reaction with a scale depth of 1.5 cm drove about twice as much dissolution (for the observed range of $k_{d,C}$ and $\Omega_{C,bw}$) as a formulation consistent with the pore water oxygen data. In addition, *Jahnke et al.* [1994] assumed that the organic carbon undergoing degradation had Redfield stoichiometry (ß = 0.77). In the previous section, ß was found to be one of the most important factors influencing the magnitude of the estimated dissolution in our sensitivity analysis, with a 70% increase in the predicted dissolution for ß = 0.77 over that predicted for ß = 0.55. These two differences in the description of the respiration reaction could lead to as much as a factor of 3 difference in the predicted metabolic dissolution. Had we restricted the value of ß in our modeling exercise to 0.69, following the results of *Anderson and Sarmiento* [1994], our estimates of the calcium and alkalinity fluxes would fall entirely within the error bars of the benthic chamber measurements.

The sensitivity of the estimated dissolution flux to the respiration reaction illustrates the necessity of accurate quantification of its depth dependence when attempting to constrain dissolution rate parameters. Without accurate, quantitative information about the depth-dependence of the respiration reaction, kinetic parameters and the proportion of metabolic dissolution cannot be assessed from flux data alone. A factor-of-two difference in dissolution flux implies orders of magnitude differences in the predicted dissolution rate constant (for these ranges in $k_{d,C}$ and $\Omega_{C,bw}$, see Figure 9). This sensitivity to the respiration rate also has implications for the atmospheric CO_2 reduction scenario presented by *Archer and Maier-Reimer* [1994], who used a simple exponential model of respiration. If the dissolution driven by metabolic CO_2 is half that predicted by the Archer and Maier-Reimer model, then the sensitivity of the atmospheric CO_2 to changes in organic carbon rain rates to the sediment will be similarly reduced (D. Archer, personal communication, 1996).

Summary

In situ electrode measurements of pore water oxygen and *p*H at three stations on the Ontong-Java Plateau in the western Equatorial Pacific imply oxygen fluxes to the sediments of 10-21 $\mu mol\ cm^{-2}\ yr^{-1}$ and calcite dissolution rates of 3.5-6 $\mu mol\ cm^{-2}\ yr^{-1}$. This dissolution rate corresponds to at least 20-40% of the calcite rain to these sediments. Dissolution driven by CO_2 produced by metabolism of organic matter in the sediments accounts for 65-80% of the total; the observed *p*H data were incompatible with any scenario excluding the effects of metabolically driven dissolution. The predicted oxygen fluxes were in good agreement with fluxes determined at one of these stations by a benthic chamber incubation experiment [*Jahnke et al.*, 1994]; calcium and alkalinity fluxes corresponding to the calcite dissolution rate predicted by the pore water model were also compatible with the chamber-determined fluxes. Our pore water oxygen profiles demonstrated that the majority of the metabolic CO_2 production was very near the interface, which allows a greater fraction to diffuse out of the pore water before it reacts with calcite. The pore water *p*H data constrain the calcite dissolution constant to 0.005%-0.16% d^{-1}, the lowest value of this parameter ever reported. This combination of kinetic parameters drives less dissolution than previous models: our representation of respiration drives about half the metabolic dissolution predicted by simple exponential models of respiration which release CO_2 at greater depths in the sediment, for the observed ranges in dissolution rate constant and bottom water saturation state.

Acknowledgements. NSF Grant OCE 9217233 funded this research. We greatly benefited from the insightful reviews of R. A. Jahnke and two anonymnous reviewers. We would like to thank J. Kaczynski for making the solid-phase organic carbon and calcite measurements.

References

Anderson, L. A., and J. L. Sarmiento, Redfield ratios of remineralization determined by nutrient data analysis, *Global Biogeochemical Cycles, 8*, 65-80, 1994.

Andrews, D., and A. Bennett, Measuring diffusivity near the sediment-water interface with a fine-scale resistivity probe, *Geochim. Cosmochim. Acta, 44*, 1955-1966, 1981.

Archer, D., The dissolution of calcite in deep sea sediments: An in situ microelectrode study, PhD thesis, Univ. of Washington, Seattle, 1990.

Archer, D., and E. Maier-Reimer, Effect of deep-sea sedimentary calcite preservation on atmospheric CO_2 concentration, *Nature, 367*, 260-263, 1994.

Archer, D., S. Emerson, and C. E. Reimers, Dissolution of calcite in deep-sea sediments: *p*H and O_2 microelectrode results, *Geochim. Cosmochim. Acta, 53*, 2831-2845, 1989.

Berelson, W. M., D. E. Hammond, J. McManus, and T. E. Kilgore, Dissolution kinetics of calcium carbonate in equatorial Pacific sediments, *Global Biogeochemical Cycles, 8*, 219-235, 1994.

Berger, W. H., and J. S. Killingley, Box cores from the Equatorial Pacific: ^{14}C sedimentation rates and benthic mixing, *Mar. Geol., 45*, 93-125, 1982.

Berger, W. H., M.-C., Bonneau, and F. L. Parker, Foraminifera on the deep-sea floor: Lysocline and dissolution rate, *Oceanol. Acta, 5*, 249-258, 1982.

Berger W. H., K., Fischer, C. Lai, and G. Wu, Ocean productivity and organic carbon flux, I, Overview and maps of primary production and export production, *Ref. Ser. q87-30*, Scripps Inst. of Oceanogr. La Jolla, Calif., 1987.

Berner, R. A.,. *Early Diagenesis--A Theoretical Approach*,Princeton Univ. Press., Princeton, N.J., 1980

Boyle, E. A., The role of vertical chemical fractionation in controlling late quaternary atmospheric carbon dioxide, *J. Geophys. Res., 93*, 15701-15714, 1988.

Broecker, W. S., The cause of the glacial to interglacial atmospheric CO_2 change: A polar alkalinity hypothesis, *Global Biogeochemical Cycles, 3*, 15-30, 1989.

Broecker, W. S., and T.-H. Peng, Gas exchange rates between air and sea, *Tellus, 26*, 21-35, 1974.

Broecker, W. S., and Peng, T.-H., The role of $CaCO_3$ compensation in the glacial to interglacial atmospheric CO_2 change, *Global Biogeochemical Cycles, 1*, 215-239, 1987.

Cai, W-J., C. E. Reimers, and T. Shaw, Microelectrode studies of organic carbon degradation and calcite dissolution at a California continental rise site. *Geochim. et Cosmochim. Acta, 59*, 497-511, 1995.

Emerson, S. R., and D. A. Archer, Glacial carbonate dissolution cycles and atmospheric P_{CO2}: A view from the ocean bottom, *Paleoceanography, 7*, 319-331, 1992.

Emerson, S. R., and M. Bender, Carbon fluxes at the sediment-water interface of the deep-sea: Calcium carbonate preservation, *J. Mar. Res., 39*, 139-162, 1981.

Farrell, J. W., and W. L. Prell, Climate change and $CaCO_3$ preservation: An 800,000 year bathymetric reconstruction from the central equatorial Pacific Ocean, *Paleoceanography, 4*, 447-466, 1989.

Hales, B., Calcite dissolution on the seafloor: An *in situ* study, Ph.D. thesis, Univ. of Washington, Seattle, 1995.

Hales, B., S. R. Emerson, and D. E. Archer, Respiration and dissolution in the sediments of the western North Atlantic: Estimates from models of *in situ* measurements of porewater oxygen and pH, *Deep-Sea Res., 41*, 695-719, 1994.

Hammond, D. E., J. McManus, W. Berelson, and T. Kilgore, Early diagenesis of organic material in equatorial Pacific sediments: Rates and kinetics, *Deep Sea Res.*, in press, 1996.

Hedges, J. I., and J. H. Stern, Carbon and nitrogen determination of carbonate-containing solids, *Limnol. Oceanogr., 29*, 657-663, 1984.

Ingle, S. E., Solubility of calcite in the ocean, *Mar. Chem., 3*, 301-319, 1975.

Jahnke, R. A., D. B. Craven, and J. F. Gaillard, The influence of organic matter diagenesis on $CaCO_3$ dissolution at the deep-sea floor, *Geochim. Cosmochim. Acta, 58*, 2799-2809, 1994.

Keir, R. S., The dissolution kinetics of biogenic calcium carbonates in seawater, *Geochim. Cosmochim. Acta, 44*, 241-252, 1980.

Keir, R. S., and R. L. Michel, Interface dissolution control of the ^{14}C profile in marine sediment, *Geochim. et Cosmochim. Acta, 57*, 3563-3573, 1993.

Li, Y. H., and S. Gregory, Diffusion of ions in sea water and and in deep-sea sediments, *Geochim. Cosmochim. Acta, 38*, 703-714, 1974.

Martin, W. R., and F. L. Sayles, $CaCO_3$ dissolution in sediments of the Ceara Rise, western equatorial Atlantic, *Geochim. Cosmochim. Acta, 60*, 243-264, 1996.

McDuff, R. E., and R. A. Ellis, Determining diffusion coefficients in marine sediments: A laboratory study of the validity of resistivity techniques, *Am. J. Sci., 279*, 666-675, 1979.

Millero, F. J., The effect of pressure on the solubility of minerals in water and seawater, *Geochim. Cosmochim. Acta, 41*, 11-22, 1983.

Morse, J. W., Dissolution kinetics of calcium carbonate in seawater, VI, The near-equilibrium dissolution kinetics of calcium carbonate-rich deep sea sediments, *Am. J. Sci., 278*, 344-353, 1978.

Mucci, A., The solubility of calcite and aragonite in seawater at various salinities, temperatures, and 1 atmosphere total pressure, *Am. J. Sci., 238*, 780-799, 1983.

Plath, D. C., K. S. Johnson, and R. M. Pytkowicz, The solubility of calcite-- probably containing magnesium-- in seawater, *Mar. Chem., 10*, 9-20, 1980.

Press, W. H., B. P., Flannery, S. A., Teukolsky, and W. T. Vetterling, *Numerical Recipes-- The Art of Scientific Computing*, Cambridge Univ. Press, New York, 1989.

Sayles, F. L., The solubility of $CaCO_3$ in seawater at 2°C based upon in situ sampled pore water composition, *Mar. Chem., 9*, 223-235, 1980.

Sayles, F. L., $CaCO_3$ solubility in marine sediments: Evidence for equilibrium and non-equilibrium behavior, *Geochim. Cosmochim. Acta, 49*, 877-888, 1985.

Sayles, F. L., and W. B. Curry, $\delta^{13}C$, TCO_2, and the metabolism of organic carbon in deep sea sediments, *Geochim. Cosmochim. Acta, 52*, 2963-2978, 1988.

UNESCO, Thermodynamics of the carbon dioxide system in seawater, Tech. Pap. Mar. Sci. 51, Paris, 1987.

Walter, L. M., and J. W. Morse, The dissolution kinetics of shallow marine carbonates in seawater: A laboratory study, *Geochim. Cosmochim. Acta, 49*, 1503-1514, 1985.

Wise, D. L., and G. Houghton, The diffusion coefficients of ten slightly soluble gases in water at 10°-60°C, *Chem. Eng. Sci., 21*, 999-1010, 1966.

Burke Hales, Lamont-Doherty Earth Observatory of Columbia University, Palisades, NY 10964. (e-mail: hales@ldgo.columbia.edu)

Steve Emerson, School of Oceanography, University of Washington, box 357940, Seattle, WA 98195-7940. (email: semerson@ocean.washington.edu)

(Received January 17, 1996; revised May 13, 1996; accepted May 14, 1996.)